Imaging the unimaginable: leveraging signal generation of CRISPR-Cas for sensitive genome imaging

Charlotte Van Tricht[1,3], Thierry Voet[2,3], Jeroen Lammertyn*[1,3], Dragana Spasic[1,3]

[1]Department of Biosystems, MeBioS-Biosensors Group, KU Leuven, 3001 Leuven, Belgium

[2]Department of Human Genetics, Laboratory of Reproductive Genomics, KU Leuven, 3000 Leuven, Belgium

[3]KU Leuven Institute for Single Cell Omics (LISCO), KU Leuven, 3000 Leuven, Belgium

*Correspondence: jeroen.lammertyn@kuleuven.be (J. Lammertyn)

C. Van Tricht: ORCID ID; LinkedIn ID; www.biosensors.be

T. Voet: ORCID ID; https://lisco.kuleuven.be

J. Lammertyn: ORCID ID; Twitter handle: @KULBiosensors; www.biosensors.be

D. Spasic: ORCID ID; Twitter handle: @KULBiosensors; www.biosensors.be

Keywords

CRISPR-Cas9, genome imaging, live-cell imaging, fixed-cell imaging, signal amplification

Abstract

Fluorescence *in situ* hybridization is the gold standard for visualising genomic DNA in fixed cells and tissues, but is incompatible with live-cell imaging and its combination with RNA imaging is challenging. Consequently, due to its capacity to bind double-stranded DNA and design flexibility, the CRISPR-Cas9 (Clustered Regularly Interspaced Short Palindromic Repeats

20 – CRISPR-associated protein 9) technology has sparked enormous interest over the past
21 decade. In this review, we will describe various nucleic acid- and protein-based (amplified)
22 signal generation methods that achieved imaging of repetitive and single-copy sequences,
23 and even single-nucleotide variants, next to highly-multiplexed as well as dynamic imaging in
24 live cells. With future progress in the field, the CRISPR-(d)Cas9-based technology promises to
25 break through as a next-generation cell-imaging technique.

26 The importance of genome imaging and its gold standard

27 The field of DNA imaging has proven instrumental in not only biomedical research but also
28 clinical practice. **Fluorescence *in situ* hybridization** (FISH) (see Glossary) revolutionized
29 classical cytogenetics –i.e. the study of chromosomes– and has been the gold standard
30 cytogenetic technique for imaging genomic DNA in fixed cells down to a few kilobases. The
31 technology played an important role in the Human Genome Project, was key in many
32 biological and biomedical discoveries [1–3], and was furthermore validated and practiced in
33 clinical diagnostics [4–6]. In FISH, double-stranded (ds) genomic DNA is first heat- or
34 chemically-denatured into single-stranded (ss) DNA [7]. The subsequent addition of
35 specifically designed ssDNA probes (i.e. FISH probes) results in their hybridization to
36 respective genomic ssDNA targets through Watson-Crick base pairing. Visualisation of the
37 FISH probes, and hence the genomic target DNA, can be achieved through labelling of FISH
38 probes (1) directly with fluorescently-labelled nucleotides or (2) indirectly through the use of
39 haptens, such as biotin [8]. Over the years, researchers have greatly improved the DNA FISH
40 technology with, for instance, hybridization to highly-stretched DNA fibers for high resolution
41 FISH (fiber-FISH) [9], next-generation synthetic oligonucleotide probes [10–12], or highly-
42 multiplexed imaging strategies [13] and the advent of simultaneous DNA and RNA ISH

43 approaches [14]. It is important to mention that the field of spatial transcriptomics, in parallel
44 to FISH for genomic DNA, has significantly progressed with the development of advanced
45 FISH-based RNA imaging technologies, such as single-molecule RNA FISH [15,16] and the
46 highly-multiplexed MERFISH version [17], which are outside the scope of this review (the
47 reader is referred to excellent reviews [18–21]). Despite these significant advancements in
48 FISH over the years, this technology comes with some intrinsic disadvantages for DNA-
49 imaging, such as the necessity for genomic dsDNA denaturation, thereby complexifying
50 simultaneous DNA and RNA imaging in multi-omics studies, and its incompatibility with live-
51 cell imaging. Therefore, less invasive approaches to image DNA in both fixed and live
52 eukaryotic cells are needed, but also novel methods for tracking DNA sequences in live cells
53 over time.

54 Pushing the boundaries in genome imaging with CRISPR-Cas9 55 technology

56 The CRISPR-Cas9 (i.e. Clustered Regularly Interspaced Short Palindromic Repeats – CRISPR-
57 associated protein 9) technology is one of the most ground-breaking biotechnologies of the
58 21st century. Ever since the development of CRISPR as a method for genome editing [22,23],
59 which was awarded the 2020 Nobel Prize in Chemistry, the research on CRISPR-Cas systems
60 has skyrocketed [24]. The CRISPR-Cas9 complex has been ingeniously engineered in
61 numerous ways to confer specific functional characteristics, enabling a myriad of applications
62 in chromatin immunoprecipitation or (epi)genome engineering [23,25,26], as well as
63 biosensing [27]. A notable example is nuclease-deficient (i.e. catalytically-dead) Cas9 (dCas9),
64 which, upon recognition, remains bound to the target dsDNA without generating dsDNA
65 breaks (DSB). As such, the CRISPR-dCas9 technology answers to the drawbacks of DNA FISH

66 since it can be easily designed to target a genomic region of interest, while not requiring global
67 dsDNA denaturation but only highly-localized DNA interrogation in the targeted sequence.
68 Ever since Chen and colleagues published the first work on CRISPR-based genome imaging
69 [28], researchers have been tinkering with the CRISPR-(d)Cas9 complex to push the
70 technology towards genome imaging of high- and low-repetitive sequences, as well as single-
71 copy sequences, and even **single-nucleotide variants** (SNV) proven so far in human and
72 mouse cells. In this review, we will cover the different CRISPR-based imaging approaches that
73 have been developed so far, while focussing on two important aspects: (1) the signal
74 generation strategy with or without signal amplification, and (2) the target detection limit in
75 terms of repetitive and single-copy sequence imaging (Figure 1, Key figure). Importantly, we
76 consider a signal to be amplified when more than one fluorescence entity is used per CRISPR-
77 (d)Cas9 entity.

78 CRISPR-based strategies for imaging repetitive sequences

79 Signal generation without amplification

80 In this section, we will discuss four elegant CRISPR-based techniques for imaging repetitive
81 sequences without signal amplification (Figure 1, upper left panel). We will discuss one of the
82 first and most established imaging strategies using dCas9 fused with fluorescent proteins
83 (hereafter referred to as CRISPR-FP), continuing with Cas9-mediated FISH (CASFISH), LiveFISH,
84 and finally CRISPR/**molecular beacon** (CRISPR/MB). CRISPR-FP has been described with
85 various fluorescent proteins, including green, blue and red fluorescent proteins (GFP, BFP and
86 RFP, respectively) or mCherry. Chen and colleagues were the first to establish this concept in
87 live cells by targeting human **telomeres** (a 5-15 kb stretch of TTAGGG repeats) with a fusion
88 protein of dCas9 and enhanced GFP (EGFP) (Figure 2A) [28]. Through optimization of the

89 single-guide RNA (sgRNA) design, they significantly increased the signal-to-background ratio
90 (S/B, i.e. ratio of mean signal intensity and mean background intensity) for imaging telomeres,
91 and two other repetitive sequences of the human mucin 4 gene (*MUC4*) (respectively ~100-
92 400 repeats and ~90 repeats, corresponding to ~45 binding sites). This multi-repeat imaging
93 was further advanced for live-cell dynamic tracking of these loci. Furthermore, dCas9 protein
94 orthologs from *S. aureus* and *S. pyogenes* (Box 1) were fused with spectrally distinct
95 fluorescent proteins (i.e. mCherry and EGFP) [29] to achieve multiplexed imaging of >30
96 repeats [30]. To expand the playing field of this imaging concept even further, Gu and
97 colleagues developed a new CARGO strategy which packaged multiple sgRNAs in a single
98 plasmid for multiplexed imaging purposes [31].

99 The optimized sgRNA design of Chen and colleagues [28] proved fundamental for much of the
100 newly developed technologies, including CASFISH – being the first CRISPR-based imaging
101 concept used in fixed cells [32]. Here, the C-terminal end of dCas9 was engineered with a
102 protein HaloTag®, creating a dCas9-Halo fusion protein (Figure 2B). By subsequent interaction
103 with the Halo ligand, modified with an organic dye (i.e. Janelia Fluor), the Halo tag covalently
104 bound its ligand, forming a signal-generating CRISPR-dCas9 complex. Through this concept,
105 Deng and colleagues initially labelled high-repetitive sequences in telomeric and
106 (peri)centromeric regions (~100s-1.000s binding sites [32]) in fixed mouse embryonic
107 fibroblast cells and mouse brain tissue sections. Furthermore, the flexibility of the Halo
108 tagging allowed for dual-colour imaging of high- and low-repetitive sequences of *MUC4* (~90
109 repeats corresponding to ~45 binding sites) and *MUC1* (~20-140 repeats) in human cells,
110 underlining its multiplexing capacity. Similarly, dCas9 fusion proteins with SNAP-tag® or CLIP-
111 tag™ were generated and linked to corresponding fluorescently-labelled ligands, which were

112 used for imaging of human repetitive telomere and centromere sequences, as well as
113 telomeres in live mouse embryos [33].

114 Whereas CRISPR-FP and CASFISH use modified dCas9 proteins, the following approaches
115 include gRNA modifications. In LiveFISH, the ribonucleoprotein (RNP) was pre-assembled
116 (prior to cell delivery) from dCas9 and a sgRNA modified with a single organic fluorophore (i.e.
117 Cy, ATTO dye) for signal generation (Figure 2C) [34]. Using this, Wang and colleagues
118 succeeded in (1) imaging high-repetitive sequences of, for instance, chromosome 13 (~350
119 repeats) in the context of Patau Syndrome detection in patient-derived live cells and (2) live-
120 cell tracking of CRISPR-Cas9-induced DSBs and resulting chromosome dynamics. Through the
121 chosen method for RNP delivery, i.e. live-cell electroporation, the researchers imaged these
122 repetitive sequences with higher S/B than the earlier-developed CRISPR-FP technology.
123 Impressively, the dCas9-based LiveFISH technology was also used in conjunction with a
124 dCas13-based CRISPR complex for RNA imaging. As such, they succeeded imaging repetitive
125 sequences at the genome and transcriptome level, while also retrieving dynamic information
126 on gene transcription.

127 Similar to LiveFISH, CRISPR/MB employed a re-engineered sgRNA, but it used an MB for signal
128 generation to increase S/B (Figure 2D) [35]. In this context, Wu and colleagues optimized a
129 sgRNA with an integrated MB target site (MTS) by assessing its insertion at various locations
130 in the sgRNA. Using the optimal design, MBs hybridized to the MTS of the sgRNA and opened
131 up, consequently generating specific signal through dissociation of the fluorophore-quencher
132 (F/Q) pair. After establishing human telomere imaging, this strategy also enabled dynamic
133 tracking of telomeres and centromeric multi-repeat sequences (~1.500-30.000 repeats [36])
134 in a two-colour multiplexed manner.

135 ## Signal generation with amplification

136 Besides the concepts for imaging repetitive sequences without signal amplification, we here
137 also discuss eight CRISPR-based imaging concepts that employed signal amplification
138 strategies (Figure 1, upper right panel). Similar to CRISPR-FP without signal amplification, Ma
139 and colleagues advanced this imaging strategy by introducing three fluorescent proteins per
140 dCas9 construct, here referred to as CRISPR-3xFP [29], thus achieving signal amplification
141 (Figure 3A). In the same publication, they also pioneered the use of dCas9 orthologs of *S.*
142 *pyogenes*, *N. meningitidis*, and *Streptococcus thermophilus* with three copies of fluorescent
143 proteins each (i.e. 3xmCherry, 3xGFP, or 3xBFP) in multiplexed colocalization on telomeres.
144 In addition, this approach (1) measured the distance between two pairs of high-repetitive
145 intrachromosomal loci and (2) probed the levels of chromatin compaction.

146 Chen and colleagues further established a novel CRISPR-FP approach with signal amplification
147 to combine genome and protein imaging. In this CRISPR-Tag concept, a DNA tag (< 850 bp)
148 was gene-edited adjacent to a protein-encoding gene of interest (Figure 3B) [37]. This DNA
149 tag contained six repeats, each harbouring four different CRISPR binding sites for DNA
150 imaging, embedded within an mCherry gene for protein imaging. Additionally, this DNA tag
151 system was combined with a split GFP system, which enabled dCas9 to recruit 14 copies of
152 GFP (i.e. dCas9-14xGFP) for amplified signal generation. For instance, the human *HIST2H2BE*
153 gene and its encoding protein were imaged throughout different cell cycle stages. In TriTag,
154 the design was optimized for smaller DNA tags with high signal-to-noise ratio (S/N, i.e. ratio
155 of the difference between mean signal intensity and mean background signal, and the
156 standard deviation of the background) towards simultaneous DNA, RNA, and protein imaging
157 [38].

158 Similarly to CRISPR-FP and CRISPR-Tag, another approach that employed protein-based signal
159 amplification is CRISPR-SunTag. The latter employed the SunTag signal generation system
160 initially developed by Tanenbaum and colleagues and involved engineering dCas9 with a
161 string of 24 GCN4 peptides (i.e. general control nonderepressible 4) to which fluorescent
162 single-chain variable antibody fragments (ScFv) could bind [39]. In their pioneering work,
163 SunTag was combined with CRISPR-dCas9 to visualize telomere dynamics in human cells.
164 Later, Ye and colleagues further optimized this imaging concept by fusing ScFv to superfolder
165 GFP (sfGFP), mNeonGreen, or three copies of mNeonGreen (3XmNeonGreen) (Figure 3C) [40].
166 In a search for increased S/B, these three signal generation constructions were used for live-
167 cell imaging of human telomeres. By comparing the signal intensity, S/B, and cell labelling
168 efficiency (i.e. signal-generated spots inside the nucleus), the mNeonGreen approach proved
169 optimal. Later, Neguembor and colleagues improved CRISPR-SunTag by using **polycistronic**
170 **vectors** to package multiple sgRNAs (i.e. Polycistronic SunTag modified CRISPR, (Po)STAC)
171 [41]. Consequently, they overcame challenges associated with individual plasmid-based
172 sgRNA delivery for multiplexing, such as variability in delivery efficiency and expression levels,
173 and reported higher S/N due to signal amplification. Notably, different metrics (S/B versus
174 S/N) are employed to characterize various imaging approaches, complexifying comparison
175 and laying bare the general need for standardized reporting in the field. Initially, CRISPR-
176 SunTag was limited to low-repeat imaging on chromosome 14 and 5 (~15 and ~21 repeats,
177 respectively). Despite the improvements, (Po)STAC only enabled high- to medium-repetitive
178 sequence imaging of *MUC4* and *MUC1* (~400 and ~20-140 repeats, respectively), although
179 multiplexed imaging was achieved both in fixed and live cells. Furthermore, the recently-
180 developed CRISPR-LIBR (i.e. CRISPR-based light-inducible background reduction) combined
181 SunTag with a light-inducible system, which increased the S/N compared to CRISPR-dCas9-

182 GFP and the original CRISPR-SunTag system [42]. Using this novel strategy, the researchers
183 imaged as low as 9-repeat sequences on chromosome 3 in human live cells.

184 In a novel approach, called CRISPR-Casilio, amplified signal generation relied on RNA
185 **aptamers** that recruit the Pumilio/FBF (PUF) RNA-binding domains of Pumilio proteins. The
186 peptide sequence of the PUF domains dictated the recognition of a specific 8-mer RNA
187 sequence (i.e. PUF binding sites (PBS)) (Figure 3D). By integrating multiple PBSs inside the
188 gRNA design, fusion proteins of PUF domains and fluorescent Clover or mRuby could bind,
189 resulting in signal amplification. In the original CRISPR-Casilio work, both telomeres and
190 centromeres were imaged in a multiplexed fashion through the use of sgRNAs containing 25
191 and 20 PBSs, respectively [43]. Interestingly, other researchers developed the all-in-one Aio-
192 Casilio where complex delivery was constituted by a single plasmid for simplification and
193 increased cell labelling efficiency [44]. After Casilio was originally coined in 2016, Hong and
194 colleagues pointed out significant non-specific signal generation in the absence of dCas9
195 when compared to CRISPRainbow (see next paragraph) and CRISPR-SunTag [45]. Therefore,
196 the same authors of the original CRISPR-Casilio recently updated their work, addressing the
197 raised signal specificity issue (see Section CRISPR-based strategies for imaging single-copy
198 sequences with signal amplification) [46].

199 To expand the multiplexing capabilities of the CRISPR genome imaging, Ma and colleagues
200 published CRISPRainbow concept employing a re-engineered sgRNA with two aptamer
201 domains: one in the gRNA stem loop and the other at the 3' end (Figure 3E) [47]. gRNAs with
202 pairs of three distinct aptamers (i.e. PUF, MS2 or PP7), each recruiting their target proteins
203 labelled with GFP, BFP, or RFP, were designed to create a combinatorial library of CRISPR
204 complexes that generated three primary (i.e. red, blue, and green) and three secondary

205 colours (i.e. cyan, magenta, and yellow). This colour-coding scheme enabled multiplexed
206 imaging of six distinct chromosome-specific repetitive sequences (>100 repeats). During the
207 same period, two other publications reported identical approaches with aptamer-engineered
208 sgRNAs for imaging telomeres and centromeres [48], and dual-colour tracking of these two
209 targets in live cells [49]. Furthermore, Fu and colleagues retrieved dynamic information from
210 centromeric repeats (> 1000 repeats) and imaged repetitive sequences (~209 repeats, but
211 only 87 sgRNA binding sites) of the A-kinase anchoring protein 6 gene (*Akap6*) in live cells
212 [50].

213 Similarly to Casilio and CRISPRainbow, Qin and colleagues developed CRISPR-16xMS2-MCP
214 with 16 copies of the MS2 aptamer embedded within and at the 3' end of its sgRNA (Figure
215 3F) [51]. Consequently, these MS2 aptamers recruited the MS2 coat protein (MCP) fused to
216 mCherry or YFP for signal amplification. This imaging strategy initially contained 14 MS2
217 copies in the 3' sgRNA end (i.e. CRISPR-14xMS2-MCP), which enabled (dynamic) imaging of a
218 low-repetitive sequence on chromosome 17 (~8 repeats), thereby achieving a great
219 improvement compared to Casilio and CRISPRainbow. Eventually, through additional sgRNA
220 engineering, the technology was pushed for single-copy imaging using the 16xMS2 form (see
221 'CRISPR-based strategies for imaging single-copy sequences with signal amplification').

222 Continuing with their CRISPRainbow work, and much like the CRISPR-16xMS2-MCP concept
223 [47], Ma and colleagues developed CRISPR-Sirius as an additional imaging strategy with signal
224 amplification(Figure 3G) [52]. To achieve better signal amplification, they optimized a sgRNA
225 design by introducing eight MS2 aptamers in the sgRNA tetraloop, and proved superior in
226 imaging repetitive sequences on chromosome 19 (~36 repeats) compared to CRISPR-14xMS2-
227 MCP. However to date, CRISPR-Sirius has been used only for dynamic imaging of distance

228 between multi-repeat loci (>20 repeats), such as **intergenic DNA regions** and pericentromeric
229 regions.

230 Last, Wang and colleagues developed a CRISPR-based imaging technique using Cas9 nickase
231 (Box 1), instead of common dCas9 [53]. In this GOLD (Genome Oligopaint via Local
232 Denaturation) FISH approach, the single-stranded cleavage activity of Cas9 nickase resulted
233 in a 3' ssDNA overhang (Figure 3H). A **DNA helicase** with 3'-5' helicase activity unwound the
234 dsDNA further downstream until halted by a blocking structure (e.g. transcription apparatus).
235 Subsequently, fluorescently-labelled FISH probes labelled the locally-unwound DNA without
236 the need for heat denaturation. Given that the use of a single CRISPR-Cas9 nickase complex
237 led to binding of multiple FISH probes, we ultimately speak of a CRISPR-based signal
238 amplification strategy. Furthermore, as Cas9 nickase both binds and cleaves the target dsDNA
239 (while dCas9 only binds its target) the technique is characterized by increased specificity and
240 S/B (compared to CASFISH [32]). Initially, imaging of repetitive sequences was established by
241 targeting *MUC4* (~400 repeats).

242 CRISPR-based strategies for imaging single-copy sequences

243 Signal generation without amplification

244 Different CRISPR-based concepts successfully achieved imaging of single-copy sequences
245 without signal amplification (Figure 1, lower left panel), more specifically CRISPR-FP, CASFISH,
246 CRISPR/dual-FRET (i.e. **Förster Resonance Energy Transfer**), and CRISPR-QD (i.e. **quantum**
247 **dot**). The CRISPR-dCas9-EGFP approach developed by Chen and colleagues (Figure 2A) was
248 further optimized for single-copy sequence imaging . Although CRISPR-FP lacks signal
249 amplification, single-copy sequence detection was achieved through gRNA tiling, whereby
250 multiple unique gRNAs are designed towards a unique genomic region of interest. Specifically,

251 73 unique sgRNAs were targeted towards *MUC4*, though imaging could already be achieved
252 with as low as 36 sgRNAs [28]. Additionally, this sgRNA set was used for dynamic tracking in
253 live cells, however at lower S/B. Furthermore, through the use of at least 485, mostly unique,
254 sgRNAs, Zhou and colleagues visualised the entire chromosome 9 and study its cell cycle
255 dynamics [54]. The set of 73 optimized sgRNAs by Chen and colleagues enabled CASFISH
256 (Figure 2B) to label the same single-copy sequence of *MUC4*. Multiplexed CASFISH was
257 achieved for multi-repeat sequences, although not yet for single-copy loci – potentially due
258 to the need for extensive sgRNA design. In SNAP-tag® and CLIP-tag™ CRISPR imaging, dynamic
259 and multiplexed imaging was achieved using 36 and 288 sgRNAs that respectively targeted
260 the human papilloma virus (HPV) integration site and myelocytomatosis (*MYC*) oncogene in
261 human cells [33].

262 Unlike CRISPR-FP and CASFISH, two strategies established solely in the context of single-copy
263 sequence imaging are CRISPR/dual-FRET and CRISPR-QD. The former stems from the
264 CRISPR/MB imaging strategy of Mao and colleagues [35] and FRET fluorophores [55]. The
265 previously optimized sgRNA-MTS design [35] included an additional MTS for hybridizing two
266 MBs with a F/Q pair for FRET (Figure 4A). Remarkably, through CRISPR/dual-FRET, the
267 researchers imaged the non-repetitive sequence of *MUC4* using only three unique sgRNAs,
268 which was a major improvement compared to 36 and 73 sgRNAs used with CRISPR-dCas9-
269 EGFP and CASFISH. Additionally, live-cell dynamics of the non-repetitive sequences of *MUC1*
270 and an intergenic DNA region were imaged through the use of three sgRNA-MTSs. Although
271 CRISPR/dual-FRET was indicated to be less amenable for multiplexing purposes due to the
272 FRET strategy, the technique demonstrated improved S/N and was superior in labelling
273 genomic loci compared to CRISPR/MB.

274 Contrary to fluorescent proteins and organic fluorophores, Ma and colleagues exploited the
275 potential of QDs, which have superior optical properties given their high quantum yield [56].
276 CRISPR-QD complexes consist of dCas9 fused to a LplA acceptor peptide (LAP) tag or biotin
277 acceptor peptide (BAP) tag (Figure 4B), which are linked to a QD inside the cell. Remarkably,
278 these QD-linking reactions were carried out in live cells whilst avoiding cytotoxic side-effects.
279 CRISPR-QD was used to diagnose HIV infections in live cells by localizing integrated HIV DNA
280 in the host genome using only two unique sgRNA designs [57]. However, this approach
281 required dual-colour QD colocalization per target as validation of signal specificity, which,
282 similar to CRISPR/dual-FRET, might preclude its multiplexing potential. To date, CRISPR-QD is
283 the strategy without signal amplification that required the least amount of unique sgRNAs to
284 image a single-copy sequence.

285 Signal generation with amplification

286 This final section covers the strategies that integrated signal amplification and realized much-
287 desired single-copy sequence imaging (Figure 1, lower right panel), such as CRISPR-SunTag,
288 CRISPR-Casilio, CRISPR-16xMS2-MCP, and GOLD FISH that have already been discussed above,
289 next to three approaches directly developed for single-copy locus imaging. As discussed in the
290 previous section, despite attempts to improve sgRNA delivery of CRISPR-SunTag (Figure 3C)
291 by enhanced delivery vectors [41], no single-copy sequence imaging had been achieved. Only
292 later when Shao and colleagues published their work on combining CRISPR-SunTag with
293 another novel plasmid assembly approach, single-copy sequence imaging was established
294 [58]. Here, 20 unique sgRNAs were cloned into a single plasmid, which enabled imaging the
295 non-repetitive sequence of the human epidermal growth factor receptor 2 (*HER2*) and *MUC4*
296 genes, while also allowing dynamic tracking of the latter.

297 Remarkably, using CRISPR-Casilio (Figure 3D) containing 15 PBSs, Clow and colleagues imaged
298 a non-repetitive sequence of *MUC4* by just one unique sgRNA design [46]. This was further
299 employed to simultaneously image two single-copy loci, allowing the study of live chromatin
300 interactions in a two-colour manner. Moreover, CRISPR-Casilio was pushed towards three-
301 colour imaging in a novel concept, coined PISCES (i.e. Programmable Imaging of Structure
302 with Casilio Emitted sequence of Signal). Here, three unique sgRNA designs were targeted to
303 adjacent non-repetitive sequences in a genome. Subsequently, using a three-colour readout,
304 the dynamic spatial organization of that genomic domain was deduced. These achievements
305 underlined the design flexibility and applicability of CRISPR-Casilio, rendering it highly
306 amenable for multiplexing. Interestingly, in a recent publication, the CRISPR-Casilio system
307 was applied in a study uncovering the cancer-related biology and cell cycle dynamics of
308 **extrachromosomal DNA** [59].

309 Initially, CRISPR-14xMS2-MCP (Figure 3F) was used for imaging multi-repeat sequences, but
310 proved unsuitable for single-copy sequences. Therefore, an alternative 16-copy version (i.e.
311 CRISPR-16xMS2-MCP) was developed with two additional MS2 aptamers internally located in
312 the sgRNA design. Consequently, Qin and colleagues imaged a single-copy sequence of the
313 *MUC4* using eight unique sgRNAs. Furthermore, to increase the sensitivity, an advanced setup
314 was used, enabling imaging of the same sequence with only four unique sgRNAs [51].

315 After having established GOLD FISH (Figure 3H) for imaging the *MUC4* repetitive sequence,
316 the technology was successfully applied to a single-copy sequence of the same gene using
317 nine unique sgRNAs and a set of 57 unique FISH probes [53]. Through two-colour GOLD FISH,
318 non-repetitive sequences of two regions on chromosome X were imaged, allowing extraction
319 of chromatin conformational interactions. Furthermore, the entire chromosome was labelled

320 and imaged through the use of 3.287 gRNAs, and 2.307 FISH probes that bound locally-
321 unwound DNA. Ultimately, GOLD FISH was successfully employed in human breast cancer
322 tissue sections for *HER2* copy number identification by single-copy sequence imaging.

323 Finally, SNP-CLING (i.e. **single-nucleotide polymorphism** CRISPR live-cell imaging) and CasPLA
324 (i.e. CRISPR-Cas9-mediated proximity ligation assay) were directly established for single-copy
325 imaging with signal amplification, and with single-nucleotide specificity [60,61]. SNP-CLING
326 relied on sgRNAs engineered with RNA-aptamers (like e.g. Casilio) for amplified signal
327 generation. The technology governed the PAM-specificity of *S. pyogenes* dCas9 to
328 discriminate between SNP-heterozygous alleles in mouse live cells, with the use of only two
329 to three unique sgRNAs. In a comprehensive study, this technology uncovered spatial inter-
330 allele distance and enabled spatiotemporal monitoring of allele dynamics in mouse live cells,
331 bringing new insights into live-cell nuclear organization.

332 Whereas SNP-CLING leveraged PAM specificity for SNP imaging, CasPLA relied on binding
333 specificity of the sgRNA seed region (i.e. a region in the gRNA sensitive to hybridization
334 mismatches) for SNV detection. Consequently, SNP-CLING is limited to SNV detection within
335 PAM sites in the target genome, while CasPLA allows more flexible application of SNV analysis
336 over the entire genome. CasPLA, as the name suggests, relied on the binding proximity of two
337 CRISPR-(d)Cas9 complexes for the initiation of a subsequent amplification reaction (i.e. **rolling**
338 **circle amplification** (RCA), Figure 5). The resulting RCA product (RCP) contained thousands of
339 copies of a known sequence to which complementary DNA probes with fluorophores bound
340 for high signal amplification. Compared to CRISPR-QD, which required localization of two
341 CRISPR complexes as a validation of signal specificity, CasPLA employed two targeted CRISPR-
342 (d)Cas9 complexes at approximately 10 nucleotides distance to achieve high signal specificity.

343 This strategy was employed to image the human NADH dehydrogenase 5 (*ND5*) gene in
344 **mitochondrial DNA** (mtDNA) using only two unique sgRNAs, and was proven to image SNVs
345 in mtDNA of cells and tissue sections. Remarkably, CasPLA was used to image the Kirsten rat
346 sarcoma viral gene (*KRAS*) in the human nuclear genome with the use of only two unique
347 CRISPR-Cas9 complexes. As such, the technique proved to be capable of detecting a single-
348 copy genomic sequence with high specificity while the sensitivity of two CRISPR-dCas9
349 complexes could distinguish between wildtype and mutated *KRAS* locus at the single-
350 nucleotide level.

351 Practical considerations for adopting CRISPR-based imaging

352 Feedback from adopters of CRISPR-based imaging indicated that repetitive-sequence imaging
353 can be easily reproduced, whereas single-copy sequence imaging remained challenging.
354 Therefore, this section addresses practical considerations regarding difficulty of engineering
355 CRISPR complexes and their cell delivery for achieving single-copy imaging. Among different
356 concepts discussed in this review, here we selected those that were established at least by
357 two independent research groups, being CRISPR-FP and CRISPR-SunTag, and concepts based
358 on aptamer-engineered sgRNAs.

359 CRISPR-FP employed fluorescent dCas9, avoiding complicated protein engineering, but also
360 lacking much-desired signal amplification [28]. Consequently, designing 10-100's sgRNAs was
361 needed to achieve single-copy sequence imaging, which was also reproduced by another
362 research group for whole-chromosome imaging [54]. Delivery of fluorescent dCas9 and sgRNA
363 was governed by lentiviral transduction, requiring plasmid cloning, lentivirus production and
364 transduction expertise for stable integration in the host cell. Although widely established for
365 live-cell imaging, this approach is labour-intensive and relies on equally efficient delivery and

366 expression of all lentiviral vectors in the host cell, thereby compromising labelling efficiency.
367 Notwithstanding the challenge in delivering multiple sgRNAs for single-copy sequence
368 imaging, the fabrication of such a sgRNA set should either be realised by (1) in-house
369 production, requiring expertise in RNA manufacturing or (2) off-the-shelf purchase, which
370 potentially involves high costs.

371 CRISPR-SunTag relied on dCas9 with a peptide array for signal amplification using antibody-
372 FP fusion proteins and was mostly reproduced independently for repetitive sequence imaging
373 [39–42]. Although requiring extensive protein engineering, the technique facilitated single-
374 copy sequence imaging by less extensive gRNA design [58]. Lentiviral transduction was used
375 for delivery of the CRISPR complex and signal-generating components [39,42], though
376 plasmid-based lipofection and electroporation was also employed by multiple groups
377 [40,41,58]. The latter is less labour-intensive as it only involves plasmid cloning and
378 transfection, yet it does not involve stable integration like lentiviral delivery while challenges
379 with achieving efficient expression remain. To overcome this, two alternative strategies were
380 used to package multiple sgRNAs in a single plasmid [41,58], one of which consequently
381 realised single-copy sequence imaging, implementing 20 unique sgRNAs in tandem.

382 Contrary to the two previous concepts, the second set of strategies discussed here relied on
383 engineered sgRNAs and is the most adopted imaging strategy of which CRISPR-Casilio,
384 CRISPRainbow, CRISPR-16MS2-MCP, CRISPR-Sirius, and SNP-CLING are five examples
385 [43,44,47–52,60]. SgRNAs, engineered with aptamers (e.g. PUF, MS2, PP7) facilitated signal
386 generation by recruiting their corresponding fluorescent fusion proteins. Two aptamers were
387 already sufficient for non-repetitive sequence imaging, and single-copy sequence imaging was
388 achieved using only one to four sgRNAs – though extensively engineered with a high number

389 of aptamers (e.g. 16 MS2 or 15 PUF) [46,51]. Furthermore, three unique sgRNAs, containing
390 only three to six aptamer domains, also enabled SNP imaging [60]. For delivery, the majority
391 relied on lentiviral transduction, yet plasmid-based delivery through lipofection was also
392 employed. Therefore, similar to CRISPR-SunTag, signal generation required efficient
393 expression of dCas9, sgRNA, and aptamer-binding proteins fused to fluorescent proteins. Yet,
394 engineered sgRNA might take up a smaller size of a vector than engineered dCas9 protein,
395 simplifying delivery of aptamer-based approaches compared to CRISPR-SunTag. Interestingly,
396 an Aio-Casilio concept provided for the first time an all-in-one solution by enabling the
397 expression of all these components through a single plasmid [44]. Although this approach
398 simplified CRISPR-Casilio delivery and increased labelling efficiency, other aptamer-based
399 approaches did not yet benefit from simplified delivery approaches and hence might still
400 suffer from the challenges that lentiviral and plasmid-based delivery of multiple different
401 vectors bring.

402 Concluding remarks and future perspectives

403 In this review, we have discussed various state-of-the-art approaches in the CRISPR-based
404 genome imaging field, while focussing on two important aspects: the target detection limit
405 (i.e. repetitive or single-copy sequences) and signal generation strategy, both in fixed and live
406 cells. Although the first CRISPR-based imaging relied on a relatively simple signal generation
407 that did not involve signal amplification, it involved sgRNA optimization, and repetitive and
408 single-copy sequence imaging [28]. As such, this pioneering work marked the inception of
409 CRISPR-based imaging and proved fundamental for many future imaging concepts.
410 Researchers quickly adopted the use of dCas9 protein orthologs to achieve CRISPR-based
411 multiplexed imaging [29,30]. With the aim of generating adequate signal intensity for genome

412 imaging and circumventing the need for extensive gRNA design, highly-repetitive genome
413 sequences (e.g. telomeres, centromeres) were the primary target for establishing new
414 imaging concepts [28,32,35]. However, to expand the applicability of CRISPR-based imaging,
415 lowering the detection limit has been the major goal in the field. This required imaging
416 strategies that yielded high S/B or S/N, while maintaining target specificity. In this context,
417 amplified signal generation by (sometimes complex) nucleic acid (NA) and protein
418 engineering has been a go-to strategy explored in many CRISPR concepts. For instance, the
419 use of in-tandem RNA aptamers [47,51] and peptides that bind F-labelled proteins [40], or
420 NA-based RCA [61] has opened up imaging capabilities towards single-copy genomic
421 sequences and SNVs. However, the field needs standardized reporting on specificity,
422 efficiency, and S/B or S/N. This can be achieved by establishing consensus in the field, but also
423 through independent comparative studies that explore the advantages and disadvantages of
424 different CRISPR-based imaging techniques in a standardized manner.

425 Despite major progress, signal amplification is not a prerequisite, nor is it a guarantee for the
426 sensitivity required for single-copy sequence imaging. As such, additional factors should be
427 taken into account when developing a new CRISPR-based imaging strategy (see Outstanding
428 questions). First, gRNA design, whether or not used to implement (amplified) signal
429 generation, has proven a crucial determinant for the success of a technology. Therefore,
430 optimization of gRNA designs might further unlock the potential of existing/future CRISPR-
431 based imaging technologies. Second, in terms of adoptability, lentiviral transduction is most
432 often used for delivery of CRISPR complexes into live cells and works robustly over a wide
433 range of different strategies. Simultaneously, the CRISPR-(d)Cas9 format and delivery
434 approach seemed to also affect the performance of new technologies. The breakthrough
435 potential of CRISPR-based imaging field lies in live-cell imaging – something which cannot be

436 achieved with standard FISH. Therefore, investigating new simplified vector packaging
437 strategies, e.g. all-in-one concepts [44] and improving strategies (e.g. transfection,
438 lipofection, electroporation) and formats (e.g. plasmid, RNP) to deliver the CRISPR complex
439 to live cells will (1) enable compatibility with and (2) facilitate further adoption of CRISPR-
440 based imaging concepts, including those for single-copy sequences. Third, the field's progress
441 might benefit from more simplified signal amplification strategies, like a recently reported
442 tracrRNA-DNA hybrid that leverages DNAzyme-based signal amplification [27]. Ultimately,
443 leveraging the design flexibility of Cas9 orthologs as well as the RNA-binding Cas12 and Cas13
444 [34], one can envision integrated CRISPR-only, multiplexed, and multi-omic cell imaging
445 strategies [62–66].

446 Acknowledgements

447 This work has received funding from the KU Leuven Research Fund through an
448 Interdisciplinary networks project (IDN/21/006 and IDN/19/039), and from The Research
449 Foundation – Flanders (FWO) (FWO G082522N and FWO G042918N). Illustrations are created
450 with Biorender.com.

451 Declaration of interests

452 The authors declare no competing interests.

453 References

454 1. Yurov, Y. B. et al. (2017) FISH-based assays for detecting genomic (chromosomal)
455 mosaicism in human brain cells. In Neuromethods (Frade, J. M. and Gage, F. H., eds.)
456 27–41, Humana Press Inc.

457 2. Wilton, L. (2002) Preimplantation genetic diagnosis for aneuploidy screening in early
458 human embryos: a review. Prenat. Diagn. 22, 512–518.

459 3. Anguiano, A. et al. (2012) Spectral Karyotyping for identification of constitutional
460 chromosomal abnormalities at a national reference laboratory. Mol. Cytogenet. 5, 3.

461 4. van Montfoort, A. et al. (2021) ESHRE PGT Consortium data collection XIX–XX: PGT
462 analyses from 2016 to 2017. Hum. Reprod. Open 00, 1–10.

463 5. Chrzanowska, N. M. et al. (2020) Use of Fluorescence In Situ Hybridization (FISH) in
464 Diagnosis and Tailored Therapies in Solid Tumors. Molecules 25, 1864.

465 6. Stender, H. (2003) PNA FISH: An intelligent stain for rapid diagnosis of infectious
466 diseases. Expert Rev. Mol. Diagn. 3, 649–655.

467 7. Kernohan, K. D. and Bérubé, N. G. (2014) Three dimensional dual labelled DNA
468 fluorescent in situ hybridization analysis in fixed tissue sections. MethodsX 1, 30–35.

469 8. Speicher, M. R. and Carter, N. P. (2005) The new cytogenetics: Blurring the
470 boundaries with molecular biology. Nat. Rev. Genet. 6, 782–792.

471 9. Ersfeld, K. (2004) Fiber-FISH: fluorescence in situ hybridization on stretched DNA.
472 Methods in Mol. Biol. 270, 395–402.

473 10. Boyle, S. et al. (2011) Fluorescence in situ hybridization with high-complexity repeat-
474 free oligonucleotide probes generated by massively parallel synthesis. Chromosome
475 Res. 19, 901–909.

476 11. Yamada, N. A. et al. (2011) Visualization of Fine-Scale Genomic Structure by
477 Oligonucleotide-Based High-Resolution FISH. Cytogenet. Genome Res. 132, 248–254.

478 12. Beliveau, B. J. et al. (2015) Single-molecule super-resolution imaging of chromosomes
479 and in situ haplotype visualization using Oligopaint FISH probes. Nature Commun. 6,
480 1–13.

481 13. Wang, S. et al. (2016) Spatial organization of chromatin domains and compartments
482 in single chromosomes. Science 353, 598–602.

483 14. Barakat, T. S. and Gribnau, J. (2014) Combined DNA-RNA fluorescent in situ
484 hybridization (FISH) to study X chromosome inactivation in differentiated female
485 mouse embryonic stem cells. J. Vis. Exp. 88, 51628.

486 15. Femino, A. M. et al. (1998) Visualization of single RNA transcripts in situ. Science 280,
487 585–590.

488 16. Raj, A. et al. (2008) Imaging individual mRNA molecules using multiple singly labeled
489 probes. Nat. Methods 5, 877–879.

490 17. Chen, K. H. et al. (2015) Spatially resolved, highly multiplexed RNA profiling in single
491 cells. Science 348, 412.

492 18. Chappell, L. et al. (2018) Single-Cell (Multi)omics Technologies. Annu. Rev. Genomics.
493 Hum. Genet. 19, 15–41.

494 19. Zhuang, X. (2021) Spatially resolved single-cell genomics and transcriptomics by
495 imaging. Nat. Methods 18, 18–22.

496 20. Moses, L. and Pachter, L. (2022) Museum of spatial transcriptomics. Nat. Methods 19,
497 534–546.

498 21. Moffitt, J. R. et al. (2022) The emerging landscape of spatial profiling technologies.

499 Nature Reviews Genetics 1–19.

500 22. Jinek, M. et al. (2012) A Programmable Dual-RNA-Guided DNA Endonuclease in
501 Adaptive Bacterial Immunity. Science 337, 816–821.

502 23. Doudna, J. A. and Charpentier, E. (2014) The new frontier of genome engineering with
503 CRISPR-Cas9. Science 346, 1258096.

504 24. You, L. et al. (2019) Advancements and Obstacles of CRISPR-Cas9 Technology in
505 Translational Research. Mol. Ther. - Methods Clin. Dev. 13, 359–370.

506 25. Pickar-Oliver, A. and Gersbach, C. A. (2019) The next generation of CRISPR–Cas
507 technologies and applications. Nat. Rev. Mol. 20, 490–507.

508 26. Xu, X. and Qi, L. S. (2019) A CRISPR–dCas Toolbox for Genetic Engineering and
509 Synthetic Biology. J. Mol. Biol. 431, 34–47.

510 27. Safdar, S. et al. (2022) Engineered tracrRNA for enabling versatile CRISPR-dCas9-
511 based biosensing concepts. Biosens. Bioelectron. 206, 114140.

512 28. Chen, B. et al. (2013) Dynamic imaging of genomic loci in living human cells by an
513 optimized CRISPR/Cas system. Cell 155, 1479–1491.

514 29. Ma, H. et al. (2015) Multicolor CRISPR labeling of chromosomal loci in human cells.
515 Proc. Natl. Acad. Sci. 112, 3002–3007.

516 30. Chen, B. et al. (2016) Expanding the CRISPR imaging toolset with Staphylococcus
517 aureus Cas9 for simultaneous imaging of multiple genomic loci. Nucleic Acids Res. 44,
518 e75.

519 31. Gu, B. et al. (2018) Transcription-coupled changes in nuclear mobility of mammalian

520 cis-regulatory elements. Science 359, 1050–1055.

521 32. Deng, W. et al. (2015) CASFISH: CRISPR/Cas9-mediated in situ labeling of genomic loci
522 in fixed cells. Proc. Natl. Acad. Sci. 112, 11870–11875.

523 33. Geng, Y. and Pertsinidis, A. (2021) Simple and versatile imaging of genomic loci in live
524 mammalian cells and early pre-implantation embryos using CAS-LiveFISH. Sci. Rep. 11,
525 12220.

526 34. Wang, H. et al. (2019) CRISPR-mediated live imaging of genome editing and
527 transcription. Science 365, 1301–1305.

528 35. Wu, X. et al. (2018) A CRISPR/molecular beacon hybrid system for live-cell genomic
529 imaging. Nucleic Acids Res. 46, e80.

530 36. Cleveland, D. W. et al. (2003) Centromeres and kinetochores: From epigenetics to
531 mitotic checkpoint signaling. Cell 112, 407–421.

532 37. Chen, B. et al. (2018) Efficient labeling and imaging of protein-coding genes in living
533 cells using CRISPR-Tag. Nature Commun. 9, 1–9.

534 38. Xu, H. et al. (2020) TriTag: an integrative tool to correlate chromatin dynamics and
535 gene expression in living cells. Nucleic Acids Res. 48, e127.

536 39. Tanenbaum, M. E. et al. (2014) A protein-tagging system for signal amplification in
537 gene expression and fluorescence imaging. Cell 159, 635–646.

538 40. Ye, H. et al. (2017) Live cell imaging of genomic loci using dCas9-SunTag system and a
539 bright fluorescent protein. Protein Cell 8, 853–855.

540 41. Neguembor, M. V. et al. (2018) (Po)STAC (Polycistronic SunTAg modified CRISPR)

541 enables live-cell and fixed-cell super-resolution imaging of multiple genes. Nucleic
542 Acids Res. 46, e30.

543 42. Hou, Y. et al. (2022) Optogenetic Control of Background Fluorescence Reduction for
544 CRISPR-Based Genome Imaging. Anal. Chem. 94, 8724–8731.

545 43. Cheng, A. W. et al. (2016) Casilio: A versatile CRISPR-Cas9-Pumilio hybrid for gene
546 regulation and genomic labeling. Cell Res. 26, 254–257.

547 44. Zhang, S. and Song, Z. (2017) Aio-Casilio: a robust CRISPR–Cas9–Pumilio system for
548 chromosome labeling. J. Mol. Histol. 48, 293–299.

549 45. Hong, Y. et al. (2018) Comparison and optimization of CRISPR/dCas9/gRNA genome-
550 labeling systems for live cell imaging. Genome Biol. 19, 39.

551 46. Clow, P. A. et al. (2022) CRISPR-mediated multiplexed live cell imaging of
552 nonrepetitive genomic loci with one guide RNA per locus. Nature Commun. 13, 1871.

553 47. Ma, H. et al. (2016) Multiplexed labeling of genomic loci with dCas9 and engineered
554 sgRNAs using CRISPRainbow. Nature Biotechnol. 34, 528–530.

555 48. Wang, S. et al. (2016) An RNA-aptamer-based two-color CRISPR labeling system.
556 Scientific Reports 6, 1–7.

557 49. Shao, S. et al. (2016) Long-term dual-color tracking of genomic loci by modified
558 sgRNAs of the CRISPR/Cas9 system. Nucleic Acids Research 44, e86–e86.

559 50. Fu, Y. et al. (2016) CRISPR-dCas9 and sgRNA scaffolds enable dual-colour live imaging
560 of satellite sequences and repeat-enriched individual loci. Nature Commun. 7, 1–8.

561 51. Qin, P. et al. (2017) Live cell imaging of low- and non-repetitive chromosome loci

562 using CRISPR-Cas9. Nature Commun. 8, 1–10.

563 52. Ma, H. et al. (2018) CRISPR-Sirius: RNA scaffolds for signal amplification in genome
564 imaging. Nat. Methods 15, 928–931.

565 53. Wang, Y. et al. (2021) Genome oligopaint via local denaturation fluorescence in situ
566 hybridization. Molecular Cell 81, 1566-1577.e8.

567 54. Zhou, Y. et al. (2017) Painting a specific chromosome with CRISPR/Cas9 for live-cell
568 imaging. Cell Res. 27, 298–301.

569 55. Mao, S. et al. (2019) CRISPR/dual-FRET molecular beacon for sensitive live-cell
570 imaging of non-repetitive genomic loci. Nucleic Acids Res. 47, e131.

571 56. Barroso, M. M. (2011) Quantum dots in cell biology. J. Histochem. Cytochem. 59,
572 237–251.

573 57. Ma, Y. et al. (2017) Live Visualization of HIV-1 Proviral DNA Using a Dual-Color-
574 Labeled CRISPR System. Anal. Chem. 89, 12896–12901.

575 58. Shao, S. et al. (2018) Multiplexed sgRNA Expression Allows Versatile Single
576 Nonrepetitive DNA Labeling and Endogenous Gene Regulation. ACS Synth. Biol. 7,
577 176–186.

578 59. Yi, E. et al. (2022) Live-Cell Imaging Shows Uneven Segregation of Extrachromosomal
579 DNA Elements and Transcriptionally Active Extrachromosomal DNA Hubs in Cancer.
580 Cancer Discov. 12, 468–483.

581 60. Maass, P. G. et al. (2018) Spatiotemporal allele organization by allele-specific CRISPR
582 live-cell imaging (SNP-CLING). Nat. Struct. Mol. Biol. 25, 176–184.

583 61. Zhang, K. et al. (2018) Direct Visualization of Single-Nucleotide Variation in mtDNA
584 Using a CRISPR/Cas9-Mediated Proximity Ligation Assay. J. Am. Chem. Soc. 140,
585 11293–11301.

586 62. Sun, N. H. et al. (2020) CRISPR-Sunspot: Imaging of endogenous low-abundance RNA
587 at the single-molecule level in live cells. Theranostics 10, 10993–11012.

588 63. Wang, M. et al. (2020) Rcasfish: Crispr/dcas9-mediated in situ imaging of mrna
589 transcripts in fixed cells and tissues. Anal. Chem. 92, 2468–2475.

590 64. de Voogt, W. S. et al. (2021) Illuminating RNA trafficking and functional delivery by
591 extracellular vesicles. Adv. Drug Deliv. Rev. 174, 250–264.

592 65. Wang, D.-X. et al. (2022) MnO 2 nanosheets as a carrier and accelerator for improved
593 live-cell biosensing application of CRISPR/Cas12a. Chem. Sci. 13, 4364–4371.

594 66. Xu, M. et al. (2022) CRISPR Cas13-Based Tools to Track and Manipulate Endogenous
595 Telomeric Repeat-Containing RNAs in Live Cells. Front. Mol. Biosci. 8.

596 67. Liu, M. Sen et al. (2019) Kinetic characterization of Cas9 enzymes. In Methods in
597 Enzymology: CRISPR-Cas Enzymes. (Bailey, S., ed.) 289–311, Academic Press Inc.

598 68. Hille, F. et al. (2018) The Biology of CRISPR-Cas: Backward and Forward. Cell 172,
599 1239–1259.

600 69. Cong, L. et al. (2013) Multiplex genome engineering using CRISPR/Cas systems.
601 Science 339, 819–823.

602 70. Mojica, F. J. M. et al. (2009) Short motif sequences determine the targets of the
603 prokaryotic CRISPR defence system. Microbiology 155, 733–740.

604 71. Friedland, A. E. et al. (2015) Characterization of Staphylococcus aureus Cas9: A
605 smaller Cas9 for all-in-one adeno-associated virus delivery and paired nickase
606 applications. Genome Biol. 16, 257.

607 72. Esvelt, K. M. et al. (2013) Orthogonal Cas9 proteins for RNA-guided gene regulation
608 and editing. Nat. Methods 10, 1116–1123.

609 73. Das, A. et al. (2022) Structural principles of CRISPR-Cas enzymes used in nucleic acid
610 detection. J. Struct. Biol. 214, 107838.

611 Box 1. CRISPR-Cas9: from biology to technology

612 The native CRISPR-Cas9 system functions as a ribonucleoprotein (RNP), comprising a Cas9
613 nuclease and a guide RNA (gRNA), which is made up of a CRISPR RNA (crRNA) and a trans-
614 activating crRNA (tracrRNA) that are partially hybridized to each other [22]. A dual process
615 governs the specific binding of CRISPR-Cas9 to its double-stranded (ds) DNA target. The
616 CRISPR-Cas9 complex first recognizes a Cas9 species-specific **protospacer-adjacent motif**
617 (PAM sequence, e.g. *NGG* for *Streptococcus pyogenes*) in the dsDNA target, and secondly
618 probes for sequence complementarity between its crRNA and the DNA target strand (i.e.
619 target protospacer sequence). The Watson-Crick base pairing between the crRNA and the
620 target protospacer is governed by the formation of an R-loop, which triggers a conformational
621 change in the CRISPR-Cas9 complex, thereby activating the cleavage activity of the two
622 CRISPR-Cas9 cleavage domains HNH and RuvC [67]. Ultimately, this process leads to a dsDNA
623 break (DSB) [68]. After scrutinizing the structure and functionality of the native CRISPR-Cas9
624 complex of *S. pyogenes*, Jinek and colleagues also demonstrated the ability of the CRISPR-
625 Cas9 complex to function with an engineered single-guide RNA (sgRNA) where the hybridized
626 regions of the crRNA and tracrRNA are linked by a linker loop (Figure IA) [22]. As such, this

627 complex could be easily designed towards any dsDNA target region of interest in the context
628 of genome engineering. Soon after, Cong and colleagues successfully demonstrated the
629 potential of the CRISPR-Cas9 technology for genome engineering in eukaryotic cells
630 specifically [69].

631 Although the first CRISPR-Cas9 systems developed for genome engineering purposes
632 originated from *S. pyogenes*, it became soon known that various Cas9 proteins from different
633 bacterial species (i.e. Cas9 orthologs) could be discriminated based on their PAM recognition
634 site [70]. For instance, the PAM sequence of the *Staphylococcus aureus* Cas9 is NNGRRT [71],
635 with R being a purine base, while an NNNNGATT PAM site is recognized by the *Neisseria*
636 *meningitidis* Cas9 protein [72].

637 Ever since the use of the CRISPR-Cas9 technology for genome editing purposes, researchers
638 have further engineered the complex to confer multiple characteristics. As such, the dCas9
639 protein (Figure IB), being deprived of the HNH and RuvC catalytic domains, offers DNA-binding
640 capacity while avoiding target DNA cleavage. Likewise, Cas9 nickase, lacks one of the two
641 catalytic cleavage domains, rendering a molecule that generates single-stranded (ss) DNA
642 nicks (Figure IC).

643 Next to Cas9 orthologs, other Cas proteins such as Cas12 and Cas13 were discovered, which
644 leverage an alternative gRNA design, and cleavage mechanism once specifically bound to the
645 target. More specifically, while CRISPR-Cas12 and -Cas13 systems specifically recognize
646 different ds/ssDNA and ssRNA targets, both respectively possess aspecific DNAse and RNAse
647 activity, so-called collateral cleavage activity, upon activation by its target molecule [73].

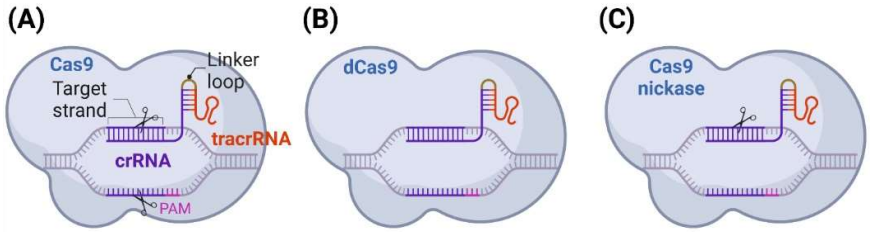

Figure I. Illustration of the quintessential Cas9 protein and two important engineered variants. (A) The CRISPR-Cas9 complex, as developed by Jinek and colleagues in 2012, which differs from the native complex by featuring a single-guide RNA (sgRNA), formed by joining the CRISPR RNA (crRNA) and trans-activating crRNA (tracrRNA) through a linker loop. The strand to which the gRNA hybridizes is called the DNA target strand (TS) whereas the complementary strand thereof is called the non-target strand (NTS). The two nuclease domains (HNH/RuvC) of the Cas9 proteins are depicted as scissors that cleave either the TS or NTS. (B) The catalytically-dead Cas9 (dCas9) protein is deprived of both catalytic cleavage domains, whereas (C) the Cas9 nickase of either of the cleavage domains.

Glossary

Aptamer: a ssDNA or ssRNA oligonucleotide which binds its ligand, such as proteins or other NAs, with high specificity.

DNA helicase: a protein enzyme that unwinds dsDNA by ATP hydrolysis.

Extrachromosomal DNA: a form of dsDNA inside and outside the nucleus of cells that does not belong to chromosomal DNA and has a circular shape.

Fluorescence in situ hybridization (FISH): a cytogenetic technique in which fluorescently-labelled probes hybridize with denatured genomic ssDNA in fixed cells or tissue samples. FISH is suitable for DNA localization studies and for uncovering genomic abnormalities ranging from numerical chromosomal changes to submicroscopic single-gene level alterations.

667 **Förster Resonance Energy Transfer (FRET):** an energy transfer mechanism, over nanometer
668 distance, from an excited donor fluorophore to an acceptor fluorophore as a consequence of
669 resonance. Such donor-acceptor fluorophores are referred to as FRET pairs.

670 **Intergenic DNA region:** the non-coding DNA region that resides between two genes.

671 **Mitochondrial DNA (mtDNA):** circularized DNA that resides in the mitochondria of eukaryotic
672 cells. Human mtDNA encompasses 16.6 kb carrying 37 genes of which 13 are protein coding
673 and 24 RNA genes. The copy number of mtDNA per cell can vary between 1000 to 100000
674 depending on the cell type.

675 **Molecular beacon (MB):** a single-stranded nucleic acid (NA) molecule with a partially self-
676 hybridized stem and a free loop structure. The distal ends of the beacon can be modified with
677 fluorophore and quencher (F/Q) pair. Under specific hybridization circumstances, the stem-
678 loop structure will open up, thereby dissociating the F/Q pair.

679 **Polycistronic vector:** a vector that contains the genetic code for more than one gene.
680 Polycistronic vectors produce a single mRNA molecule that leads to the expression of multiple
681 proteins.

682 **Protospacer-adjacent motive (PAM)**: a Cas9-species-specific multi-nucleotide sequence (e.g.
683 NGG for *Sp.* Cas9), positioned next to the non-target strand, which is specifically recognized
684 by the CRISPR-(d)Cas9 complex prior to binding.

685 **Quantum dot (QD):** nanoparticle with a specific crystal structure that possesses unique
686 optical properties resulting from its small size.

687 **Rolling circle amplification (RCA):** a NA amplification technique, which is triggered by the
688 hybridization of a single-stranded padlock probe to a NA target sequence of interest. The

689 padlock probe is circularized by ligation and a primer is hybridized. DNA polymerase elongates
690 the primer, creating a long linear product with thousands of copies of the padlock probe.

691 **Single-nucleotide polymorphism (SNP):** a type of single-nucleotide variation that occurs in
692 germline genomic DNA and is present in at least 1% of the species' population.

693 **Single-nucleotide variant (SNV):** a general term for an alteration in a DNA sequence that
694 involves the variation of one single nucleotide.

695 **Telomere:** a region of repetitive sequences that is situated at the end of linear chromosomes
696 in eukaryotic cells. Telomeres protect the chromosomal DNA, enable complete replication of
697 genetic material throughout the cell cycles, and can be involved in chromosome movement
698 and positioning.

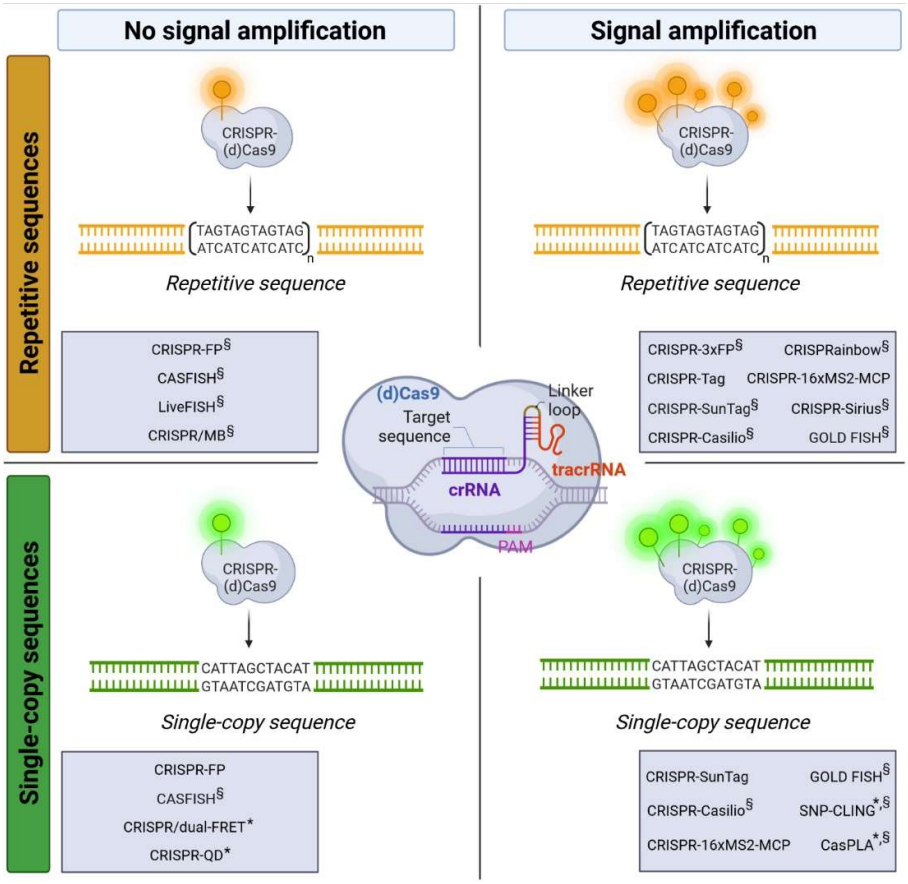

Figure 1. Key figure. Schematic overview of subjects discussed in this review. The four panels correspond to the four sections of this review. The upper two panels describe CRISPR technologies that realized imaging of repetitive sequences either with or without the implementation of signal amplification. The two lower panels describe the CRISPR-based imaging strategies that achieved imaging of single-copy sequences, likewise with or without signal amplification. The DNA sequences depicted in the four panels are arbitrary sequences and are purely for illustrative purposes. *Strategies that were directly established for imaging of single-copy sequences. §Strategies where multiplexed imaging has been achieved. Abbreviations: FP, fluorescent protein; CASFISH, Cas9-mediated fluorescence in situ hybridization; MB, molecular beacon; GOLD FISH, genome oligopaint via local denaturation FISH; FRET, Förster resonance energy transfer; QD, quantum dot; CasPLA, CRISPR-Cas9-mediated proximity ligation assay; SNP-CLING, single-nucleotide polymorphism CRISPR live

711 cell imaging ;dCas9, catalytically-dead Cas9; crRNA, CRISPR RNA; tracrRNA, trans-activating

712 crRNA. References for main concepts: [28,29,32,34,35,37,40,46,47,51–53,55,57,60,61].

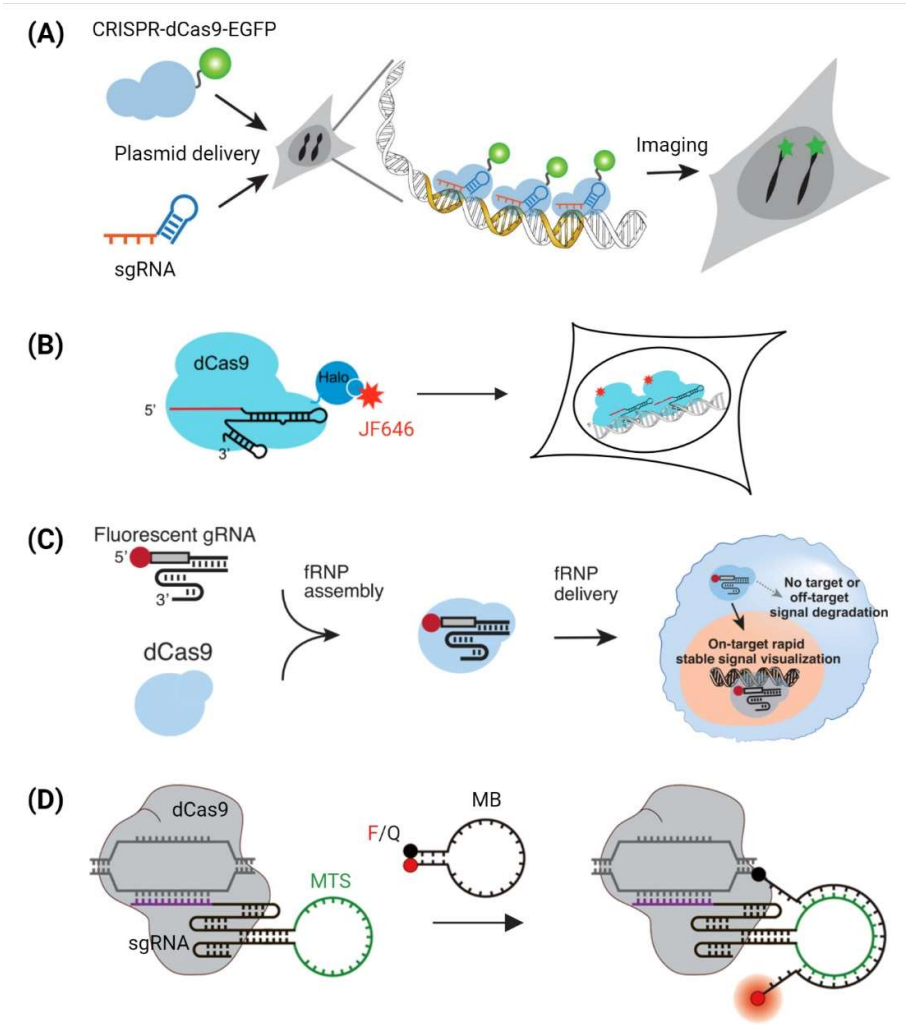

713 **Figure 2. Schematic overview of the signal generation strategies for imaging repetitive**

714 **sequences without signal amplification.** (A) In CRISPR-dCas9-(E)GFP, a fusion protein of

715 catalytically-dead Cas9 (dCas9) and enhanced (E) GFP (i.e. dCas9-(E)GFP), together with a

716 single-guide RNA (sgRNA), form a functional and fluorescent CRISPR-dCas9 complex for

717 specific signal generation. (B) In CASFISH, the CRISPR-dCas9 ribonucleoprotein (RNP) contains

718 a Halo tag for binding its fluorophore (F)-labelled Halo ligand. (C) In LiveFISH, an F-labelled

719 sgRNA and dCas9 protein form a fluorescent RNP (fRNP) that is responsible for signal

720 generation upon target binding. (D) The CRISPR/MB (i.e. molecular beacon) approach relies

721 on an engineered sgRNA with MB target site (MTS, green) (i.e. sgRNA-MTS) and a dCas9
722 protein. Subsequent binding of fluorophore and quencher (F/Q)-labelled MBs results in signal
723 generation. In (A), plasmid-based transfection was used to deliver the CRISPR-(d)Cas9
724 complexes to live cells. In (D) Lentiviral transduction was used to generate cell lines that stably
725 express the CRISPR-(d)Cas9 complexes. In (B), the CRISPR-(d)Cas9 complexes were delivered
726 as RNP in fixed cells, while in (C) and (D), electroporation was used for delivery of CRISPR
727 complex and MBs, respectively. Abbreviations: JF646, Janelia fluor 646. Illustrations adapted
728 with permission from [28,32,34,35].

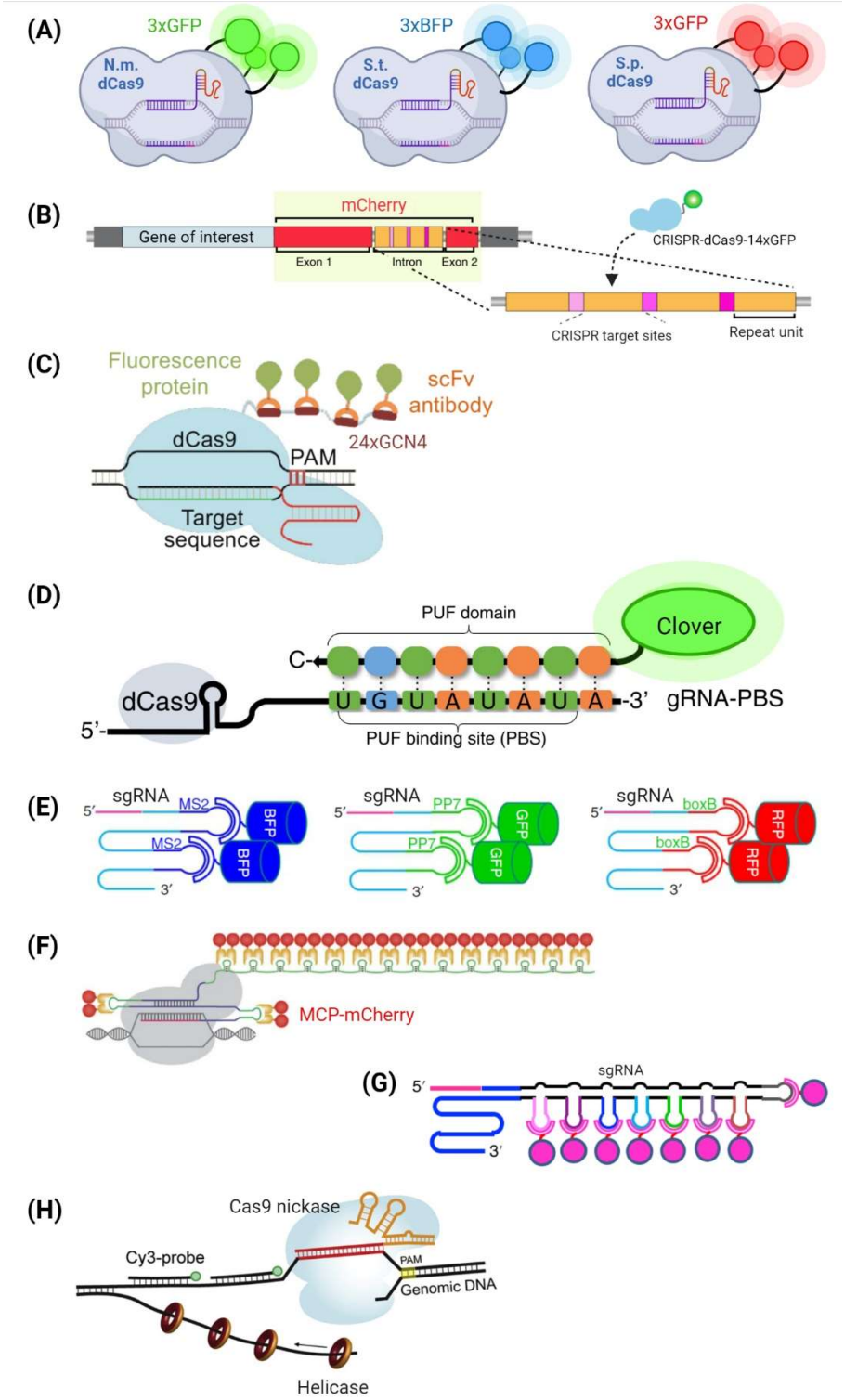

Figure 3. Schematic overview of the signal generation strategies for imaging repetitive sequences with signal amplification. (A) In CRISPR-3xFP, catalytically-dead Cas9 (dCas9) protein orthologs of *N. meningitidis*, *S. thermophilus*, and *S. pyogenes*, were engineered to

732 contain three copies of green, blue, or red fluorescent protein (GFP, BFP, RFP) each. (B) In
733 CRISPR-Tag, the DNA tag was inserted next to a gene of interest (grey) by CRISPR gene editing.
734 The tag consists of an mCherry-encoding gene (red) with repeat units (orange) in its intron
735 that contain multiple CRISPR target sites to which the CRISPR-dCas9-14xGFP complexes
736 bound. (C) The CRISPR-SunTag is composed of a 24xGCN4 (i.e. general control
737 nonderepressible 4) peptide string (red) to which F-labelled antibodies (scFv, orange) bind.
738 (D) The sgRNA of the CRISPR-Casilio complex contains up to 25 Pumilio/FBF (PUF) binding sites
739 (PBSs) to which F-labelled PUF domains bind. (E) In CRISPRainbow, modified single-guide
740 RNAs (sgRNAs) contain pairs of MS2, PP7 or boxB aptamers that bind fluorophore (F)-labelled
741 fusion proteins of MS2 coat protein (MCP), PP7 coat protein, or λ N-peptide, respectively. (F)
742 In CRISPR-16xMS2-MCP, 16 MS2 aptamers are included in the sgRNA which bind F-labelled
743 MCP proteins. (G) In the CRISPR-Sirius complex, eight MS2-MCP interactions are employed in
744 its gRNA. (H) GOLD FISH relies on cleavage activity of Cas9 nickase and the local DNA-
745 unwinding activity of helicase for subsequent FISH (i.e. fluorescence in situ hybridization)
746 probe hybridization (i.e. Cy3-probe). In concepts (A), (C), (D), and (E), plasmid-based
747 transfection was used to deliver the CRISPR-(d)Cas9 complexes to live cells. In (B), (D), (F), and
748 (G), lentiviral transduction was used to generate cell lines that stably express the CRISPR-
749 (d)Cas9 complexes. In (H), the CRISPR-Cas9 nickase complex was delivered to fixed and
750 permeabilized cells as a ribonucleoprotein (RNP). Illustrations adapted with permission from
751 [29,37,40,46,47,51–53].

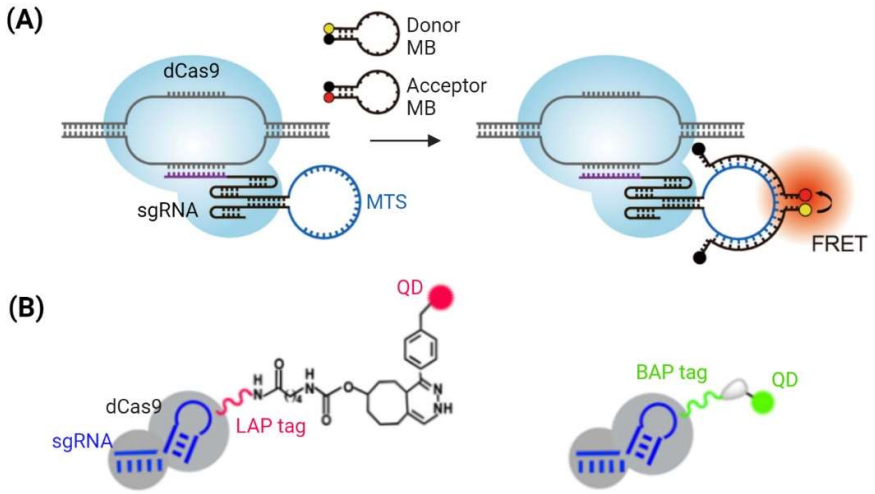

Figure 4. Schematic of the strategies for imaging single-copy sequences without signal amplification. (A) In CRISPR/dual-FRET (i.e. Förster Resonance Energy Transfer), the single-guide RNA (sgRNA) was engineered to contain a molecular beacon (MB) target site (MTS, blue) to which two MBs with fluorophore and quencher (F/Q) pair bind. These two MBs, called donor (yellow) and acceptor (red) MB form a FRET pair for signal generation upon hybridization to the MTS. (B) In CRISPR-QD (i.e. quantum dots), the catalytically-dead Cas9 (dCas9) is fused to an LplA acceptor peptide (LAP) tag or biotin acceptor peptide (BAP) tag. By the respective use of a ligase or streptavidin-biotin chemistry, two QDs with distinct fluorescent properties are linked to these tags through a ligase or through streptavidin-biotin chemistry. (B) used plasmid-based transfection for the delivery of the CRISPR-dCas9 complexes. In (A), lentiviral transduction was used to deliver CRISPR complexes in live cells. Additionally, (A) and (B) used electroporation and transfection for delivery of the MBs and QDs, respectively. Illustrations adapted with permission from [55,57].

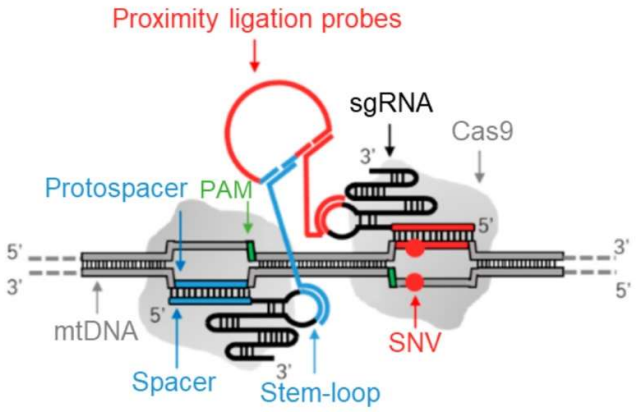

765 **Figure 5. Schematic of the imaging strategy that was directly developed for single-copy**
766 **sequence imaging with signal amplification.** In CasPLA (i.e. proximity ligation assay), binding
767 of two adjacently-targeted CRISPR complexes to, for instance, mtDNA is followed by the
768 hybridization of a set of proximity ligation probes, which bind to the stem-loop structure of
769 the two corresponding single-guide RNAs (sgRNAs). Ultimately, after hybridization of the
770 probe set and DNA ligation, a circular DNA molecule is formed which is fundamental for a
771 rolling circle amplification reaction. The CRISPR-Cas9 complex is pre-assembled in vitro, after
772 which it is delivered to the fixed and permeabilized cells, followed by delivery of the various
773 nucleic acid probes for signal generation, and detection at the SNV level. Additional
774 abbreviations: PAM, protospacer-adjacent motif; mtDNA, mitochondrial DNA; SNV, single-
775 nucleotide variant. Illustration adapted with permission from (61).